Coherent laser excitation of ^{137}Ba and ^{138}Ba

Kai-Shue Lam

Department of Physics, California State Polytechnic University, Pomona, California 91768

Computations are carried out for the $^1S(6s^2)$-$^1P(6s,6p)$ coherent laser excitation of ^{137}Ba and ^{138}Ba in a magnetic field. Results are presented for both the steady-state and time-dependent excited-state populations of the Zeeman-split magnetic sublevels. The quantum-statistical Liouville-equation approach (for the reduced density matrix) is compared to the rate-equations approach. Significant differences are found between these, due to the interference between strongly overlapping lines (especially for ^{137}Ba). The time-evolution profiles indicate that the ^{137}Ba transient time is much longer than that of ^{138}Ba.

I. INTRODUCTION

In a wide variety of experiments aimed at the detailed study of excited atomic (molecular) systems, laser radiation has long been used for the preparation of specific excited states [1,2]. Most of these experiments only require lasers of moderate power (approximately in the milliwatts to watts range) so that strong-field phenomena, such as multiple-photon absorption, dressed-state spectroscopy, and ultrafast nonresonant radiative collisions, etc., can be ignored. Under these conditions, the dynamics of the atomic (molecular) system interacting with the laser radiation can be understood readily in terms of the field-free states. A basic problem is then the determination of the time evolution of excited-state populations as the matter system is pumped in a collisionless environment by the laser for a time period long in comparison with typical excitation and decay times. A knowledge of the time profile of these populations is critical for the understanding of secondary processes occurring on the excited states, such as electron scattering, electron-impact ionization, photodissociation, photoionization, and various charge-transfer processes.

In this paper we investigate theoretically the coherent laser excitation of ^{137}Ba and ^{138}Ba from the ground manifold $^1S(6s^2)$ to the excited manifold $^1P(6s6p)$ in the presence of a magnetic field. The excitation of the Zeeman-split magnetic sublevels arising from the fine structure (^{138}Ba) and the hyperfine structure (^{137}Ba) exhibits interesting temporal coherences and steady-state power-broadening effects due to overlapping resonances that are of crucial importance in the interpretation of experimental results on excited-state processes. Data for Ba in a collisionless environment already exist for electron-impact ionization [3,4] and superelastic electron scattering [5] from the ^1P excited manifold.

The physically appealing and conceptually simple rate-equations approach has often been successfully used in many applications on the interpretation of excitation spectra [6]. It fails, however, to describe temporal coherences due to quantum superposition [2,7,8]. In this work we will use a nonrelativistic quantum-electrodynamical (QED) model to describe the laser-atom interaction and a

quantum-statistical density-matrix approach [2] based on the Liouville-space formalism [9] to treat the dynamics of the coherent excitation. This approach will adequately describe temporal coherences in the presence of energy and/or phase relaxation due to spontaneous emission [10]. Our treatment is based on the Schrödinger picture, where the time evolution of the reduced density matrix for the atomic subsystem is directly calculated. A parallel treatment based on the Heisenberg picture calculates instead the time evolution of the radiation field [11] and atomic operators [12].

Section II summarizes the theory on which our calculations are based. The main result is the Liouville equation for the reduced density matrix ρ_A [Eq. (12) and Table I]. We also discuss the transition from the Liouville Equation to the rate equations [Eq. (21) and Table II]. Section III presents details and results of our calculations for the σ and π pumping of the Ba systems. We will demonstrate significant differences between the density-matrix and rate-equations approaches (Figs. 6, 7, and 10), interference effects due to overlapping resonances (Fig. 7), and different transient time scales in the time-evolution profiles of the excited-state populations of the two isotopic species (Figs. 10–12). Section IV concludes the paper with a discussion of the numerical results.

II. THE LIOUVILLE EQUATION FOR THE REDUCED DENSITY MATRIX AND THE CORRESPONDING RATE EQUATIONS

Our QED model consists of a single-mode laser in the Fock representation interacting with a multilevel atom capable of spontaneous decay. The atomic levels consist of a ground-state manifold (g), an excited-state manifold (e), and metastable bath manifold (b). The single laser mode is chosen with frequency ω_L approximately resonant between the g and e levels but far off resonance between the b and e levels. We thus exclude absorption from the metastable bath states back to the excited manifold after spontaneous decay from e to b. Figure 1 shows schematically the atomic levels with the allowed radiative processes in our model.
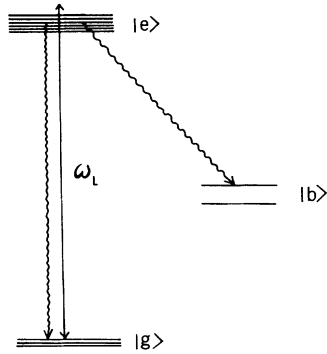
FIG. 1. Schematic atomic energy-level diagram for the QED model of Eqs. (1)–(4). The solid line represents absorption and stimulated emission of a laser photon of energy $\hbar\omega_L$. Wavy lines represent spontaneous emission.

We assume the g and e states are dipole coupled and use the rotating-wave approximation (RWA) [13]. The total Hamiltonian in second-quantized form can then be written as

$$H = H_{\text{atom}} + H_{\text{field}} + H_i , \qquad (1)$$

where

$$H_{\text{atom}} = \sum_g \varepsilon_g c_g^\dagger c_g + \sum_e \varepsilon_e c_e^\dagger c_e , \qquad (2)$$

$$H_{\text{field}} = \sum_k \hbar\omega_k a_k^\dagger a_k , \qquad (3)$$

$$H_i = -\boldsymbol{\mu}\cdot\mathbf{E}$$
$$= \hbar \sum_{e,d,k} [g_{ed}^k c_e^\dagger c_d a_k + (g_{ed}^k)^* a_k^\dagger c_d^\dagger c_e] , \qquad (4)$$

with

$$g_{ed}^k \equiv -i\hat{\boldsymbol{\varepsilon}}_k \cdot \mathbf{D}_{ed} \left| \frac{2\pi\omega_k}{\hbar V} \right|^{1/2} , \qquad (5)$$

$$\mathbf{D}_{ed} \equiv \langle e|\boldsymbol{\mu}|d \rangle . \qquad (6)$$

In Eqs. (4)–(6), d denotes either the g or b states. In Eq. (2) ε_g and ε_e denote the atomic energy levels, and c_i ($c_i^\dagger$) the atomic annihilation (creation) operators. In Eq. (3), k labels the field mode (wave vector $\hat{\mathbf{k}}$ and polarization vector $\hat{\boldsymbol{\varepsilon}}_k$), ω_k is the field frequency of the k mode, and $a_k^\dagger$ (a_k) represent creation (annihilation) operators for photons of the k mode. Equation (4) gives the interaction Hamiltonian within the dipole approximation and the RWA. $\boldsymbol{\mu}$ is the atomic dipole moment operator and $\mathbf{E}$ is the electric-field operator (with constant amplitude). The first term in the sum on the right-hand side of Eq. (4) describes absorption by the ground manifold. The second term describes stimulated and spontaneous emission from the excited to the ground manifold, and spontaneous decay from the excited manifold to the bath. In Eq. (5), V is the quantization volume.

The RWA amounts to including only those processes where absorption is accompanied by atomic excitation and emission by atomic deexcitation. Under the RWA, the Hilbert subspace spanned by the dressed

atomic states $|g,N_L\rangle$, $|g,N_L-n;k_{i_1},\ldots,k_{i_n}\rangle$, $|e,N_L-n;k_{i_1},\ldots,k_{i_{n-1}}\rangle$, and $|b,N_L-1;k_1\rangle$, where $1 \le n \le N_L$ and $k_i \ne L$, is then invariant under H. In the above notation, L labels the single laser mode, N_L is the number of photons in that mode, and k_i represents a single photon in the arbitrary k_i mode. The coupling between the dressed states is shown in Fig. 2.

We consider only laser powers such that the Rabi frequencies are comparable to the spontaneous-decay rates (Einstein A coefficients $\sim 10^8$ s^{-1}). Then $N_L \gg 1$; but for typical laser-atom interaction times of interest (on the order of 100 atomic lifetimes), the cascading towards lower N_L is still completely negligible. In these situations only the states $|e,N_L-1\rangle$, $|g,N_L\rangle$, $|g,N_L-1;k_1\rangle$, and $|b,N_L-1;k_1\rangle$ are effectively coupled by H_i. Physically $|e,N_L-1\rangle$ will represent the excited atomic states in a laser field with the number of photons in the L mode $< N_L$. Thus absorption from all the $|g,N_L-1;k_1\rangle$ states will replenish $|e,N_L-1\rangle$ and the sequence of states in Fig. 2 (in principle progressing all the way down to $|g,0;k_1,\ldots,k_{N_L}\rangle$) can be truncated at $|g,N_L-1;k_1\rangle$. To simplify notation we will denote our truncated (but still infinite set of) basis states by

$$|e\rangle \equiv |e,N_L-1\rangle , \qquad (7a)$$

$$|g\rangle \equiv |g,N_L\rangle , \qquad (7b)$$

$$|k_g\rangle \equiv |g,N_L-1;k_1\rangle , \qquad (7c)$$

and

$$|k_b\rangle \equiv |b,N_L-1;k_1\rangle . \qquad (7d)$$

The full density matrix $\rho_{ij}(t)$, where i,j refer to the basis states in Eq. (7), can be partitioned as follows:

$$\rho(t) = \begin{bmatrix} \rho_A & \rho_{AB} \\ \rho_{BA} & \rho_{BB'} \end{bmatrix} , \qquad (8)$$

where A denotes the atomic subsystem (states labeled by e or g), and B the bath of spontaneous decay channels (states labeled by k_g or k_b) [c.f. Eq. (7)]. We seek the equation of motion (Liouville equation) for ρ_A, the reduced density matrix for the atomic subsystem.
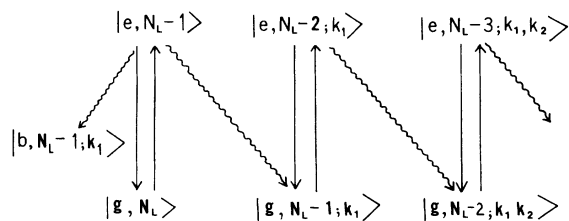
A convenient procedure consists in applying the resol-

FIG. 2. Coupling scheme between the basis states in an invariant subspace of the total Hamiltonian H given by Eq. (1). Upward solid arrows represent absorption, downward solid arrows represent stimulated emission, and wavy arrows represent spontaneous emission. See text for an explanation of the state labels.

TABLE I. The time-evolution matrix $(L_0+\mathcal{L}_1)$. For details on the notation see Eqs. (13)–(20). The sign convention for the decay coherence term (proportional to the square root of the product of Einstein A coefficients) is as follows: $+$ $(-)$ is used when the corresponding dipole moment matrix elements have the same sign (opposite sign).

	g_3g_4	g_3e_4	e_3g_4	e_3e_4
g_1g_2	$\omega_{g_1g_2}\delta_{g_1g_3}\delta_{g_2g_4}$	$-\Omega_{e_4g_2}\delta_{g_1g_3}$	$\Omega_{e_3g_1}\delta_{g_2g_4}$	$\pm i\delta m_{31}m_{42}(A_{e_3g_1}A_{e_4g_2})^{1/2}$
g_1e_2	$-\Omega_{e_2g_4}\delta_{g_1g_3}$	$\delta_{g_1g_3}\delta_{e_2e_4}(\Delta_{e_2g_1}-i/2N_e\tau_t)$	0	$\Omega_{e_3g_1}\delta_{e_2e_4}$
e_1g_2	$\Omega_{e_1g_3}\delta_{g_2g_4}$	0	$\delta_{g_2g_4}\delta_{e_1e_3}(-\Delta_{e_1g_2}-i/2N_e\tau_t)$	$-\Omega_{e_4g_2}\delta_{e_1e_3}$
e_1e_2	0	$\Omega_{e_1g_3}\delta_{e_2e_4}$	$-\Omega_{e_2g_4}\delta_{e_1e_3}$	$\delta_{e_1e_3}\delta_{e_2e_4}(\omega_{e_1e_2}-i/N_e\tau_t)$

vent method with the appropriate projection operators to the Fourier transform of $\rho(t)$ [14]. The resulting equation (exact) is [4]

$$\dot{\rho}_A(t)=-iL\rho_A(t)$$
$$-\int_0^t dt' L_1 e^{-i[L_0+(1-D)L_1]t}(1-D)L_1$$
$$\times\rho_A(t-t') , \tag{9}$$

where the Liouville operator L is defined by

$$L\rho=[H,\rho] , \tag{10}$$

and L_0 (L_1) corresponds to the unperturbed (interaction) Hamiltonian. The projection operator D projects onto the atomic subspace: $D\rho=\rho_A$. Equation (9) clearly describes memory effects. The Markovian (memory-erasing) approximation consisting of the steps

$$\int_0^t dt'\to\int_0^\infty dt' \tag{11a}$$

and

$$\rho_A(t-t')\to\rho_A(t) \tag{11b}$$

is then applied to yield finally the Liouville equation [4]

$$\dot{\rho}_A(t)=-i(L_0+\mathcal{L}_1)\rho_A(t) , \tag{12}$$

where L_0 is diagonal and the entire time-evolution matrix $L_0+\mathcal{L}_1$ is time independent. Its specific form is given in Table I. The notation used in this table is explained as follows: The resonance frequencies ω_{ij} are given by

$$\omega_{ij}=(E_i-E_j)/\hbar , \tag{13}$$

the detunings Δ_{eg} are

$$\Delta_{eg}=\omega_L-\omega_{eg} , \tag{14}$$

and the Rabi frequencies Ω_{eg} are

TABLE II. Time-evolution matrix (L_2) for the rate equations. The absorption and stimulated emission rates β_{eg} are given by Eq. (22).

	g_2	e_2
g_1	$-\delta_{g_1g_2}\sum_e\beta_{eg_1}$	$\beta_{e_2g_1}+A_{e_2g_1}$
e_1	$\beta_{e_1g_2}$	$-\delta_{e_1e_2}\left[\sum_g(\beta_{e_1g}+A_{e_1g})+\sum_b A_{e_1b}\right]$

$$\Omega_{eg}=\mathrm{sgn}(D_{eg})(\hat{\varepsilon}_L\cdot\hat{\mathbf{e}}_{\Delta m})\left[\frac{B_{eg}U_L}{2\pi}\right]^{1/2}$$
$$(\Delta m=0,\pm1) . \tag{15}$$

In (15), Δm is the change in magnetic quantum number for the dipole transition $(g\to e)$ and $\hat{\varepsilon}_L$ is the laser-polarization unit vector (perpendicular to wave vector of laser). The unit vectors in circular basis are

$$\hat{\mathbf{e}}_\pm=\mp\frac{1}{\sqrt{2}}(\hat{\mathbf{e}}_x\mp i\hat{\mathbf{e}}_y) , \tag{16a}$$

$$\hat{\mathbf{e}}_0=\hat{\mathbf{e}}_z , \tag{16b}$$

U_L is the laser energy density, the Einstein A and B coefficients are given by

$$B_{eg}=\frac{3\pi^2c^3A_{eg}}{\hbar\omega_{eg}^3} , \tag{17}$$

$$A_{eg}=\frac{4D_{eg}^2\omega_{eg}^3}{3\hbar c^3} , \tag{18}$$

N_e is the total number of excited states in the ^1P manifold, and

$$\frac{1}{\tau_t}=\frac{1}{\tau_g}+\frac{1}{\tau_b} , \tag{19}$$

in which τ_g is the lifetime for $e\to g$ decay and τ_b is the lifetime for $e\to b$ (metastable bath) decay, and
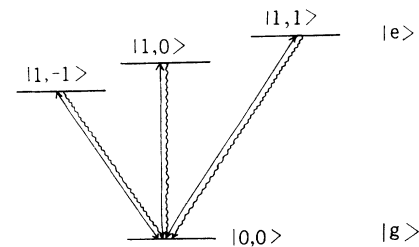

FIG. 3. Pumping and decay scheme for the Zeeman-split magnetic sublevels of the ^{138}Ba $^1S(6s^2)\to{}^1P(6s,6p)$ transition. The individual sublevels are designated by $|F,m_F\rangle$. Solid arrows represent absorption and stimulated emission. Wavy arrows represent spontaneous emission. (The Zeeman-splittings as shown are grossly exaggerated.)

TABLE III. Resonance energy levels $\nu = E/h$ for the Zeeman-split magnetic sublevels of the $^1P(6s6p)$ excited manifold of ^{137}Ba and ^{138}Ba used in the present calculations. Values for ^{138}Ba are referenced to $\nu(1,-1)=0$, those for ^{137}Ba to $\nu(\frac{5}{2},-\frac{5}{2})=0$. The splittings are created by a magnetic field of ~ 93 G (Ref. [4]).

	F'	m_F'	$\nu(F',m_F')$ (MHz)
^{138}Ba	1	-1	0
		0	130
		1	260
^{137}Ba	$\frac{5}{2}$	$-\frac{5}{2}$	0
		$-\frac{3}{2}$	36.03
		$-\frac{1}{2}$	77.67
		$\frac{1}{2}$	127.26
		$\frac{3}{2}$	188.49
		$\frac{5}{2}$	260.40
	$\frac{3}{2}$	$-\frac{3}{2}$	305.58
		$-\frac{1}{2}$	324.04
		$\frac{1}{2}$	348.82
		$\frac{3}{2}$	414.12
	$\frac{1}{2}$	$\frac{1}{2}$	613.07
		$-\frac{1}{2}$	687.45

$$m_{ij} = \Delta m(e_i \leftarrow g_j) . \tag{20}$$

Dipole moment matrix elements D_{eg} for specific transitions $(e \leftarrow g)$ of the Ba systems under study are given in the next section [Eqs. (23) and (24)].

The rate equations for the diagonal elements of ρ_A (populations) are obtained from the Liouville equation for ρ_A [Eq. (12)] by another round of projection and Markovian approximation. The result is [4]

$$\dot{\rho}_D = L_2 \rho_D , \tag{21}$$

where the time-evolution matrix L_2 for the atomic populations (ρ_D) is given in Table II. The absorption and stimulated emission rates β_{eg} in this table are given by the Lorentzians [4]

FIG. 4. Level scheme for the hyperfine Zeeman-split magnetic sublevels of the ^{137}Ba $^1S(6s^2) \rightarrow {}^1P(6s,6p)$ transition. The numbers directly above the levels denote m_F. (Zeeman splittings are grossly exaggerated.)
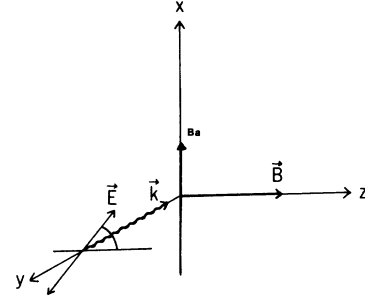

FIG. 5. Possible geometry of experimental setup for the σ (π) pumping of Ba. B represents the magnetic field responsible for the Zeeman splitting of the excited hyperfine states. k represents the propagation direction (wave vector) of the laser beam. E represents the polarization direction (on the xz plane).

$$\beta_{eg} = \frac{A_{eg}\Omega_{eg}^2}{(\omega_L - \omega_{eg})^2 + A_{eg}^2/4} . \tag{22}$$

In practice one can phenomenologically insert arbitrary line-shape functions (of ω_L) for β_{eg} to incorporate inhomogeneous as well as homogeneous broadening. Our calculations use Eq. (22).

The rate equations for populations contain less spectral (time coherence) information than the corresponding Liouville equation for the reduced density matrix ρ_A. The information (memory) loss becomes more severe as the amount of overlap between the atomic resonances increases. In the next section we will show the differences between these two approaches.

III. THE CALCULATIONS

For both ^{137}Ba and ^{138}Ba, we label the atomic states with the hyperfine spectroscopic designation (F, m_F) for uniformity of notation, even though $I = 0$ for ^{138}Ba. Thus we consider dipole transitions between the $^1S(6s^2)$ manifold with hyperfine magnetic sublevels labeled by $|\alpha = [(6s^2), L = 0, S = 0]; J = 0, I; F, m_F\rangle$ and the $^1P(6s,6p)$ manifold with the corresponding labeling $|\alpha' = [(6s,6p), L' = 1, S' = 0]; J' = 1, I; F', m_F'\rangle$. For ^{138}Ba $(I = 0)$ the ground manifold consists of only one magnetic sublevel $|\alpha;(0,0);(0,0)\rangle$ while the excited manifold consists of three Zeeman-split magnetic sublevels $|\alpha';(1,0);(1,m_F'=0,\pm1)\rangle$. The $^1S \rightarrow {}^1P$ transition for ^{138}Ba thus constitutes a four-level system with a pumping and spontaneous-decay scheme illustrated in Fig. 3. For ^{137}Ba $(I = \frac{3}{2})$ the ground manifold consists of four hyperfine magnetic sublevels $|g_i\rangle = |\alpha;(0,\frac{3}{2});(\frac{3}{2},m_F = \pm\frac{3}{2},\pm\frac{1}{2})\rangle$, and the excited manifold consists of 12 Zeeman-split hyperfine magnetic sublevels

$$|e_i\rangle = \begin{vmatrix} \alpha';(1,\frac{3}{2});(F'=\frac{5}{2},m_F'=\pm\frac{5}{2},\pm\frac{3}{2},\pm\frac{1}{2}) \\ (F'=\frac{3}{2},m_F'=\pm\frac{3}{2},\pm\frac{1}{2}) \\ (F'=\frac{1}{2},m_F'=\pm\frac{1}{2}) \end{vmatrix} .$$

The level scheme for the ^{137}Ba $^1S \rightarrow {}^1P$ transition is illustrated in Fig. 4. The optical transition $^1S \rightarrow {}^1P$ is ~ 2.4 eV $\sim 5.76 \times 10^{14}$ Hz and we consider Zeeman splittings of < 700 MHz brought about by a magnetic field of ~ 100 G (see Table III). In practice spontaneous emission from the ^1P manifold also populates the lower-lying bath manifolds ^3P, ^1D, and ^3D (between ~ 1.1 and ~ 1.7 eV above

the ^1S ground state). This is relatively insignificant compared with emission to the ^1S manifold (branching ratio $\sim 1{:}300$), [15] and will be ignored in our calculations, although the formalism includes it. The $\sigma(\Delta m_F = \pm 1)$, $\pi(\Delta m_F = 0)$, and σ plus $\pi(\Delta m_F = 0, \pm 1)$ pumping schemes will be considered. These can be realized, for example, by a crossed atomic beam–laser magnetic-field experiment [3] in which the component beams are at right angles to each other and the laser is linearly polarized, as shown in Fig. 5.

The dipole matrix elements D_{eg} can be obtained with the help of the Wigner-Eckart theorem. We have [16]
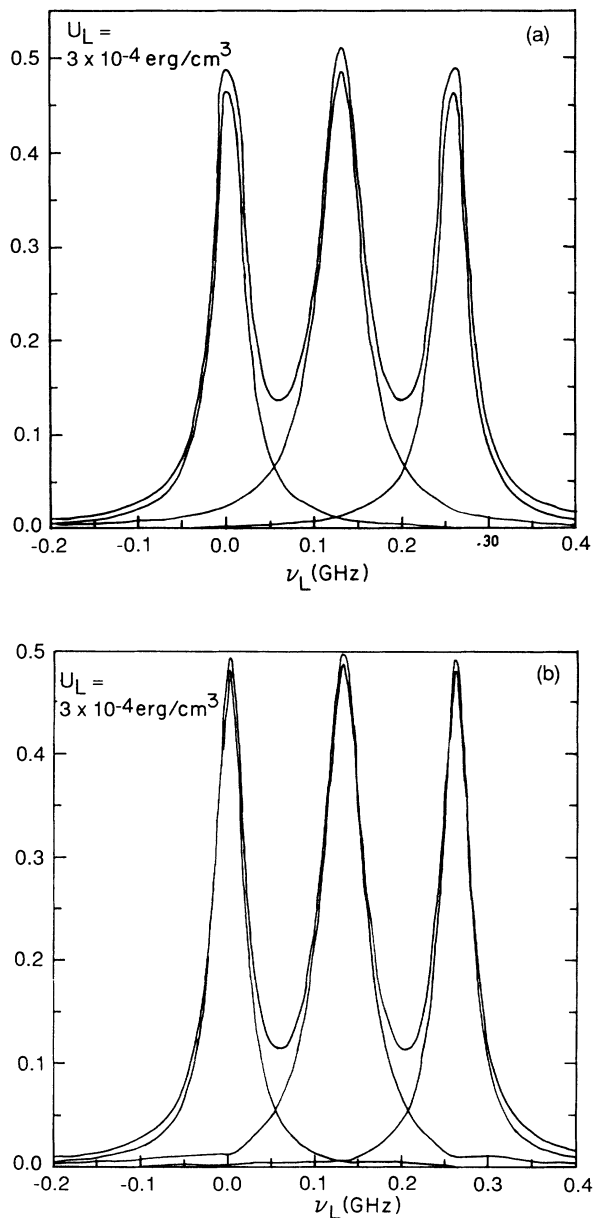
FIG. 6. Density-matrix (a) and rate-equations (b) steady-state excited-state populations of the ^{138}Ba $^1S \rightarrow {}^1P$ transitions (shown in Fig. 3) as functions of laser frequency for $\sigma + \pi$ pumping. Zero frequency is at the $|F=1, m_F = -1\rangle$ level. Positions of all excited Zeeman-split magnetic sublevels are 0.13 GHz apart. U_L is the laser energy density. The curves in each figure include the individual excited-state populations and the total excited-state population.
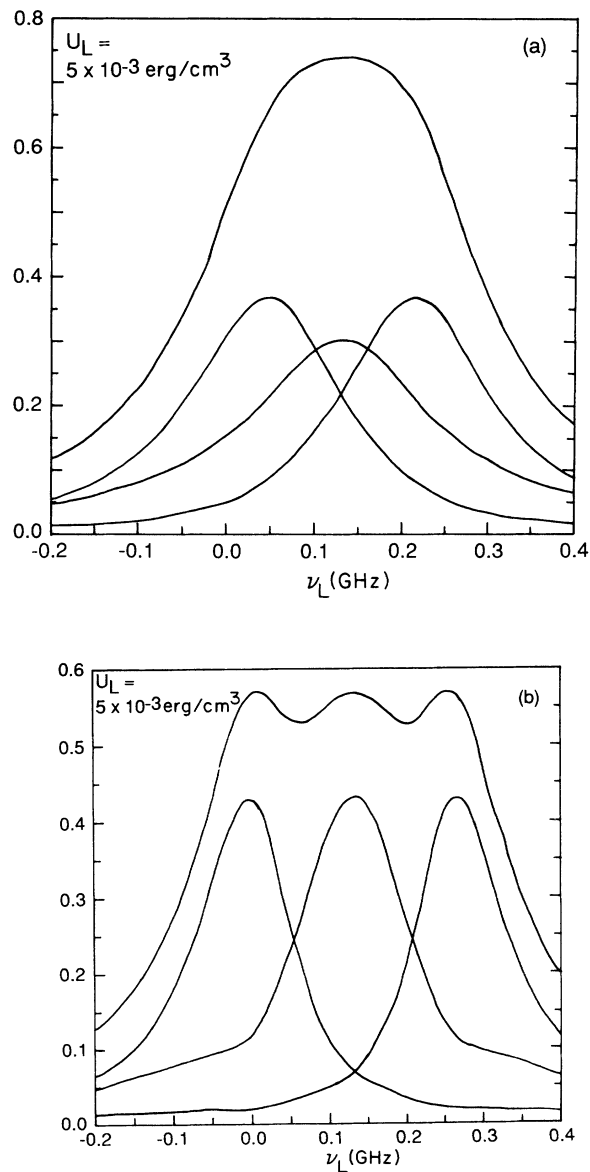
FIG. 7. The same results as in Fig. 6 for a higher laser energy density: from density matrix (a) and rate equations (b). Note that interference effects due to overlapping resonances are quite apparent in this figure. (See Fig. 6 caption.)

$$\langle [(6s6p), L', S']; J'I; F'm_F' | D_{\Delta m}^{(1)} | [(6s^2), L, S]; JI; Fm_F \rangle$$

$$= (-1)^{F'-m_F'+J'+I+F+L'+S'+J} [(2F'+1)(2F+1)(2J'+1)(2J+1)]^{1/2} \delta_{S'S}$$

$$\times \begin{bmatrix} F' & 1 & F \\ -m_F' & \Delta m & m_F \end{bmatrix} \begin{Bmatrix} F' & 1 & F \\ J & 1 & J' \end{Bmatrix} \begin{Bmatrix} J' & 1 & J \\ L & S' & L' \end{Bmatrix} \langle (6s6p)L' || D^{(1)} || (6s^2)L \rangle .$$

(23)

This leads to the following expressions for the $^1S \rightarrow {}^1P$ dipole transitions:
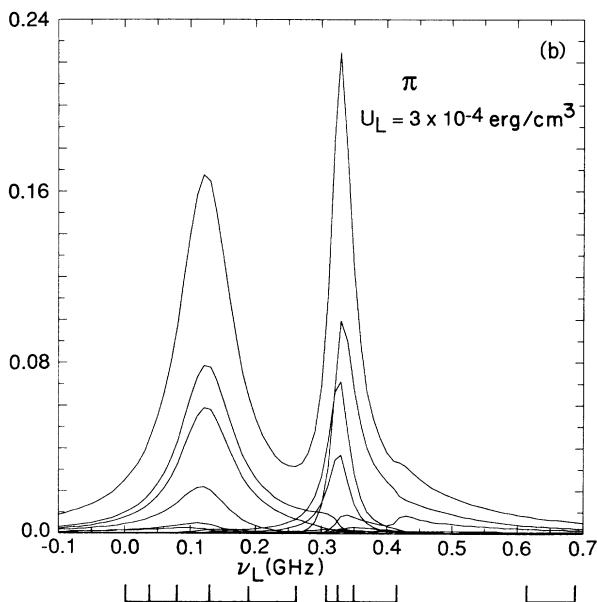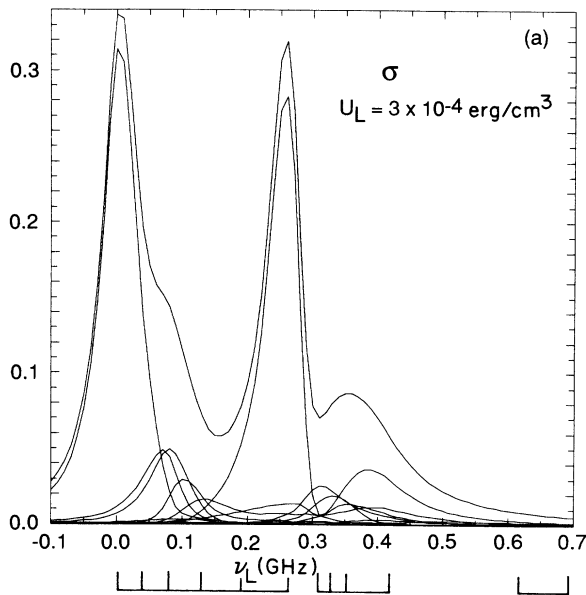
FIG. 8. Density-matrix steady-state excited-state populations of the ^{137}Ba $^1S \rightarrow {}^1P$ transitions (Fig. 4) as functions of laser frequency, for σ pumping (a) and π pumping (b). Zero frequency is at the $|F = \frac{5}{2}, m_F = -\frac{5}{2}\rangle$ level. Positions of the Zeeman-split magnetic sublevels (see Table III) are indicated. U_L is the laser energy density. The curves in each figure include the individual excited-state population and the total excited-state population. Note the uneven shifts and broadening of the individual excited-state resonances.
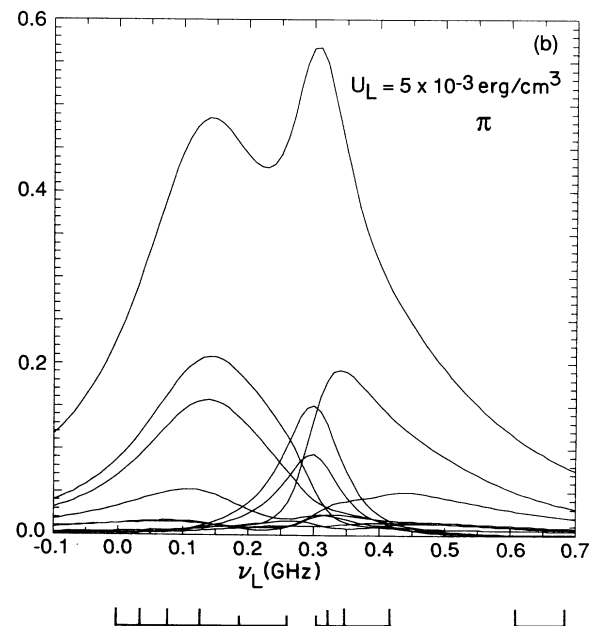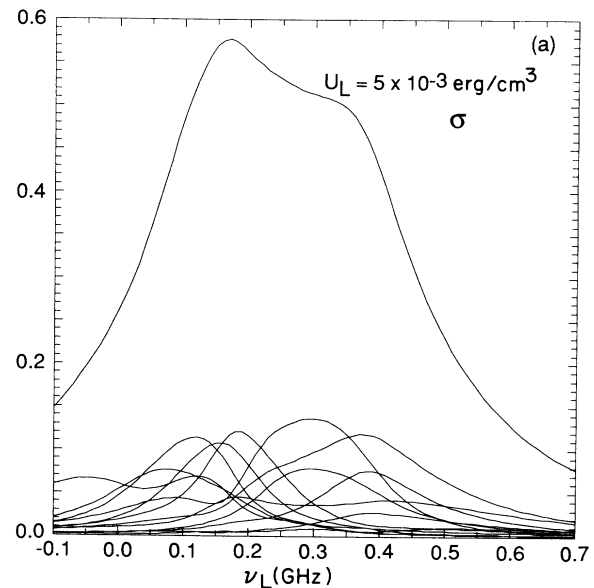
FIG. 9. Same results as in Fig. 8 for a higher laser energy density: σ pumping (a) and π pumping (b). (See Fig. 8 caption.)

$$D_{eg} = \begin{cases} \dfrac{M}{\sqrt{3}} \, , \quad {}^{138}\text{Ba} & \text{(24a)} \\[2em] (-1)^{2F'-m_F'+3/2} \left[\dfrac{(2F'+1)}{3} \right]^{1/2} \begin{bmatrix} F' & 1 & \frac{3}{2} \\ -m_F' & \Delta m & m_F \end{bmatrix} M \, , \quad {}^{137}\text{Ba} & \text{(24b)} \end{cases}$$

where M is the reduced matrix element

$$M = \langle (6s\,6p)L' = 1 || D^{(1)} || (6s^2)L = 0 \rangle \, . \tag{25}$$

M can be determined in terms of empirical ${}^1P$ lifetimes τ_g (for ^{138}Ba) and τ_g' (for ^{137}Ba) by

$$\frac{4\omega_{eg}^3}{3\hbar c^3} M^2 = \frac{1}{4\tau_g'} = \frac{1}{\tau_g} \, . \tag{26}$$

Standard matrix techniques [17] are used for the solutions of the Liouville equation and the rate equations. All eigenvalues and eigenvectors are obtained with the EISPACK matrix eigensystem routines [18]. Determinants are evaluated with the LINPACK linear algebra routines [19]. Numerical inputs for the present calculations are listed as follows:

$$\omega_{eg} = 2\pi(5.76 \times 10^{14}) \text{ s}^{-1} \, , \tag{27}$$

$$\tau_g = 8.37 \times 10^{-9} \text{ s}^{-1} \, , \tag{28}$$

$$(\rho_A)_{g_i g_j}(0) = \delta_{ij}/N_g \, , \tag{29a}$$

$$(\rho_A)_{ge}(0) = (\rho_A)_{eg}(0) = (\rho_A)_{e_i e_j}(0) = 0 \, , \tag{29b}$$

$$(\rho_D)_{g_i}(0) = 1/N_g \, , \tag{30a}$$

$$(\rho_D)_{e_i}(0) = 0 \, , \tag{30b}$$

where N_g is the total number of states in the ${}^1S$ manifold. With respect to the geometry of Fig. 5

$$\hat{\varepsilon}_L = \begin{cases} \hat{z} & (\pi \text{ pumping}) \\ \hat{x} & (\sigma \text{ pumping}) \\ \dfrac{1}{\sqrt{2}}(\hat{x}+\hat{z}) & (\sigma + \pi \text{ pumping}) \end{cases} \tag{31}$$

Table III gives the energy values for the Zeeman-split magnetic sublevels.

Figures 6–9 present computed results for steady-state excited-state populations as functions of laser frequency, while Figs. 10–12 show time-evolution profiles of total excited-state populations (sum of all Zeeman-split level populations in the ${}^1P$ manifold). In Figs. 6, 7, and 10 density-matrix results are compared with rate-equations results for $\sigma + \pi$ pumping of ^{138}Ba. Figures 8, 9, 11, and 12 show density-matrix results for ^{137}Ba, for σ and π pumping separately.

IV. DISCUSSION

Figures 6, 7, and 10 for ^{138}Ba results show clearly the similarities and differences between the Liouville equation (density-matrix) and rate-equation approaches. For short times (much less than steady-state time scales), the differences are manifested by the presence of large Rabi oscillations in the density-matrix excited-state populations, in contrast to the steady buildup of the rate-equation populations. For on-resonance frequencies, the rate-equation populations correspond roughly to the
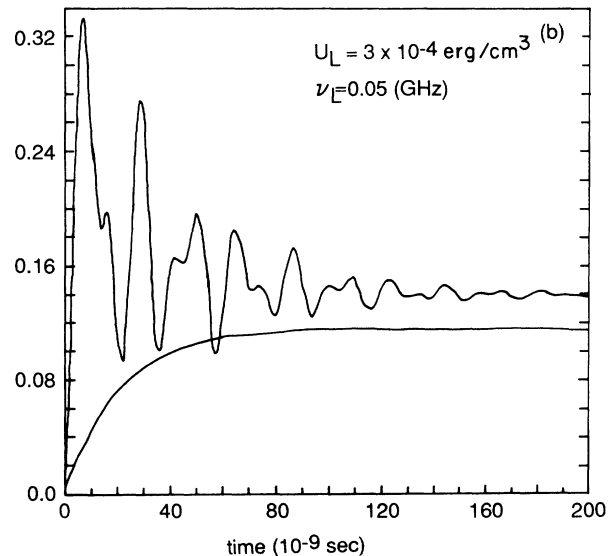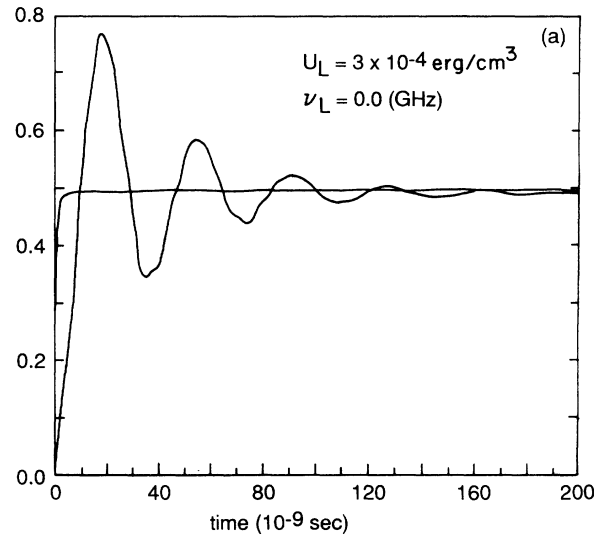
FIG. 10. Time-evolution profile ($\sigma + \pi$ pumping) of the total excited-state population of the ^{138}Ba ${}^1S \rightarrow {}^1P$ transitions (shown in Fig. 3), for two laser frequencies ν_L. Zero laser frequency is at the $|F=1, m_F = -1\rangle$ level and the excited levels are 0.13 GHz apart (see Table III). U_L is the laser energy density. Each figure compares the density-matrix results (curves with Rabi oscillations) to the rate-equation results (curves with steady buildup).

density-matrix populations averaged over the Rabi oscillations [Fig. 10(a)]. But this is no longer true as one moves away from resonance [Fig. 10(b)]. If one is only interested in the steady-state ($t \to \infty$) populations, however, our results indicate that the two approaches are comparable when the laser energy density is low enough so that the individual atomic resonances do not overlap significantly (Fig. 6). With the increase in laser energy density, power broadening causes strong overlap and interference between the resonances. The Liouville-equation approach is capable of describing these interference effects by incorporating phase information carried

by the time evolution of the off-diagonal density-matrix elements of ρ_A and predicts shifts and broadening of the individual resonances that are significantly different from those predicted by the rate equations (Fig. 7). These differences, as discussed previously, result from the fact that, on passing from the Liouville equation to the rate equations, a Markovian approximation is introduced which erases memory and thus spectral information.

The Zeeman-split hyperfine spectroscopy of the ^{137}Ba leads to strongly overlapping resonances, even for relatively low laser powers. Thus interference effects due to power broadening are expected to be much more
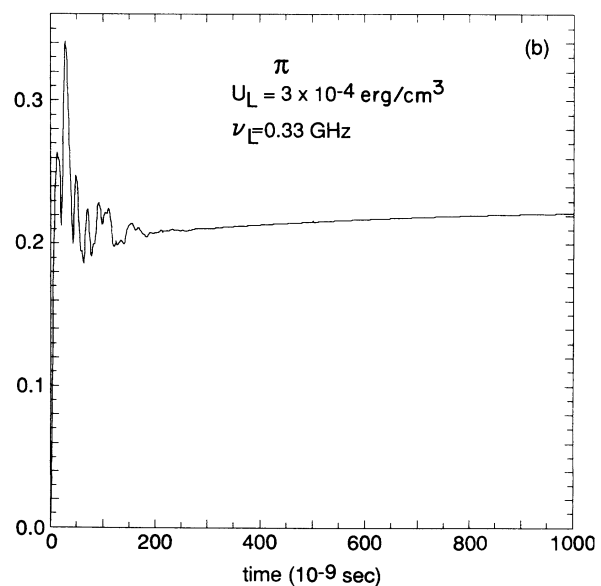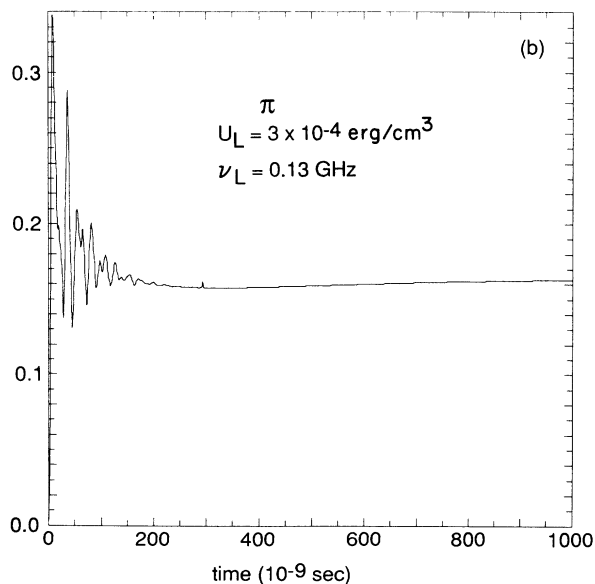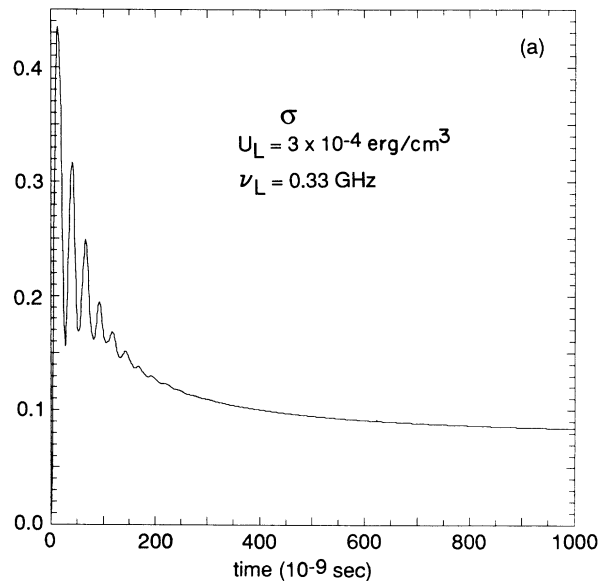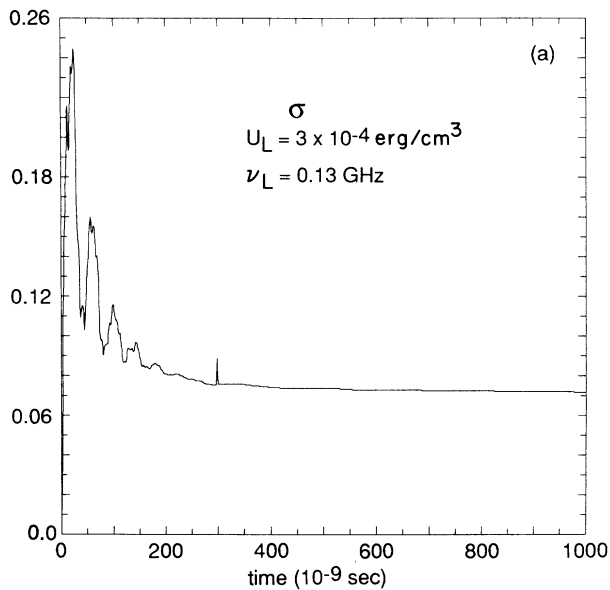

FIG. 11. Density-matrix time-evolution profiles of the total excited-state population of the ^{137}Ba $^1S \to ^1P$ transitions (Fig. 4), for σ pumping (a) and π pumping (b). U_L is the laser energy density and ν_L is the laser frequency. Zero laser frequency is at the $|F = \frac{5}{2}, m_F = -\frac{5}{2}\rangle$ level.

FIG. 12. Same results as in Fig. 11 for a different laser frequency. (See Fig. 11 caption.)

significant than in the case of ^{138}Ba. This is revealed strikingly in Figs. 8 and 9, which show the shifts and broadening of the individual Zeeman-split resonances as well as the total excited-state populations.

Time-evolution profiles for ^{137}Ba, shown in Figs. 11 and 12, indicate that it takes significantly longer for the odd isotope excited-state populations to approach steady-state values: $\sim$ 500 ns for ^{137}Ba compared to $\sim$ 200 ns for ^{138}Ba. Rabi oscillations, however, disappear at $\sim$ 200 ns for both the even and odd isotope cases. These time characteristics should be important for the interpretation of time-resolved experimental data.

We conclude by mentioning that for direct comparison with experimental data our formalism and computations would have to be appropriately modified to accommodate specific experimental situations, such as Doppler broadening, time dependence of laser power, etc. These, however, present no difficulties in principle.

ACKNOWLEDGMENTS

[1] N. Andersen, J. W. Gallagher, and I. V. Hertel, Phys. Rep. **165**, 1 (1988).

[2] B. W. Shore, *The Theory of Coherent Atomic Excitation* (Wiley-Interscience, New York, 1990), Vols. I and II.

[3] S. Trajmar, J. C. Nickel, and T. Antoni, Phys. Rev. A **34**, 5154 (1986).

[4] K. S. Lam, S. Trajmar, J. C. Nickel, and P. W. Zetner, Jet Propulsion Laboratory Report No. JPL D-7111-A (unpublished).

[5] D. F. Register, S. Trajmar, G. Csanak, S. W. Jensen, M. A. Fineman, and R. T. Poe, Phys. Rev. A **28**, 151 (1983).

[6] U. Hefter and K. Bergmann, in *Atomic and Molecular Beam Methods,* edited by G. Scoles, associate editors D. Bassi, U. Buk, and D. Lainé (Oxford University Press, Oxford, 1988), p. 193; K. Bergman, *ibid.,* p. 293.

[7] W. E. Lamb, Jr., in *Laser Photochemistry, Tunable Lasers, and Other Topics,* edited by S. F. Jacobs, M. Sargent III, M. O. Scully, and C. T. Walker, Physics of Quantum Electronics Vol. 4 (Addison-Wesley, Reading, MA 1976), p. 403.

[8] P. M. Farrell, W. R. MacGillivray, and M. C. Standage, Phys. Rev. A **37**, 4240 (1988).

[9] U. Fano, in *Boulder Lectures in Theoretical Physics* (Interscience, New York, 1961), Vol. III, p. 217.

[10] G. S. Agarwal, *Quantum Statistical Theories of Spontaneous Emission and Their Relation to Other Approaches,* Springer Tracts in Modern Physics Vol. 70 (Springer-Verlag, New York, 1974).

[11] J. R. Ackerhalt and J. H. Eberly, Phys. Rev. D **10**, 3350 (1974).

[12] W. R. MacGillivray and M. C. Standage, Phys. Rep. **168**, 1 (1988); Aust. J. Phys. **43**, 401 (1990).

[13] P. W. Milonni and J. H. Eberly, *Lasers* (Wiley, New York, 1988).

[14] R. Zwanzig, Physica **30**, 1109 (1964).

[15] G. K. Gerke and B. A. Bushaw, Phys. Rev. A **37**, 1502 (1988).

[16] See, for example, M. Weissbluth, *Atoms and Molecules* (Academic, New York, 1978).

[17] M. W. Hirsch and S. Smale, *Differential Equations, Dynamical Systems, and Linear Algebra* (Academic, New York, 1974).

[18] B. T. Smith, J. M. Boyle, J. J. Dongarra, B. S. Garbow, Y. Ikebe, V. C. Klema, and C. B. Moler, *Matrix Eigensystem Routines-EISPACK Guide,* 2nd ed. (Springer-Verlag, New York, 1976); B. S. Garbow, J. W. Boyle, J. J. Dongarra, and C. B. Moler, *Matrix Eigensystem Routines-EISPACK Guide Extension* (Springer-Verlag, New York, 1977).

[19] J. J. Dongarra, C. B. Moler, J. R. Bunch, and G. W. Steward, *LINPACK Users Guide* (Society for Industrial and Applied Mathematics, Philadelphia, 1979).